IEEE Access
Multidisciplinary | Rapid Review | Open Access Journal

Received March 4, 2018, accepted April 3, 2018, date of publication April 11, 2018, date of current version May 9, 2018.

Digital Object Identifier 10.1109/ACCESS.2018.2825429

Channel-Coded Physical-Layer Network Coding With OFDM Modulation

LING FU XIE[1,2], IVAN WANG-HEI HO[3], (Member, IEEE), ZHEN HUI SITU[3], LU LU[4], (Member, IEEE), AND WEIDANG LU[5], (Member, IEEE)

[1]Faculty of Electrical Engineering and Computer Science, Ningbo University, Ningbo 315211, China
[2]Science and Technology on Communication Networks Laboratory, CETC, Shijiazhuang 050081, China
[3]Department of Electronic and Information Engineering, The Hong Kong Polytechnic University, Hong Kong
[4]Key Laboratory of Space Utilization, Technology and Engineering Center for Space Utilization, Chinese Academy of Sciences, Beijing 100864, China
[5]College of Information Engineering, Zhejiang University of Technology, Hangzhou 310023, China

Corresponding author: Ling Fu Xie (xiel0002@ntu.edu.sg)

This work was supported in part by the National Natural Science Foundation of China under Project 61601254 and Project 61501390, in part by the K. C. Wong Magna Fund in Ningbo University, and in part by the Science and Technology on Communication Networks Laboratory of CETC under Project 614210401050217. The work of I. W.-H. Ho and Z. H. Situ was supported in part by the Early Career Scheme established under the University Grant Committee of the Hong Kong Special Administrative Region, China, under Project 25200714, and in part by The Hong Kong Polytechnic University under Project G-YBK6, Project G-YBR2, and Project G-YBXJ.

ABSTRACT This paper addresses the carrier frequency offset (CFO) problem in OFDM modulated physical-layer network coding (PNC) operated in a two-way relay channel (TWRC). CFO, caused by node-motion induced Doppler shifts and/or asynchronous oscillators, induces inter-carrier interference (ICI) between OFDM subcarriers and hence, degrades PNC performance. To mitigate the CFO/ICI effect in PNC, this paper considers channel-coded PNC and focuses on the receiver design at the relay. CFO compensation, signal detection, and channel decoding are the three basic signal processing blocks at the relay node. For the latter two, we consider both a joint and a separate design. For the joint design, we construct a factor graph to integrate channel coding with ICI, and then, propose a scheme based on belief propagation. For the separate design, two low-complexity schemes differing in channel decoding are proposed. Our simulation results, using repeat-accumulate channel codes, reveal that (1) a CFO compensation approach that amounts to positioning the relay's oscillator frequency at the middle of the received frequencies from the two end nodes is bit error rate (BER)-optimal for all the three schemes; (2) the joint design is superior at low SNR and/or high CFO levels; and (3) more importantly, with the joint design, for low-to-medium CFO levels, the BER of the channel-coded PNC is comparable with that of traditional point-to-point communications without CFO, thus manifesting itself as a promising technique in OFDM modulated TWRC with practical CFO constraints.

INDEX TERMS Belief propagation, carrier frequency offset, inter-carrier interference, OFDM, physical-layer network coding.

I. INTRODUCTION

Physical-layer Network Coding (PNC) is a promising technique in relay networks [1]. A typical scenario where PNC has found great success is Two-Way Relay Channel (TWRC), as shown in Fig. 1. In TWRC, two end nodes A and B want to exchange packets X_A and X_B via a relay R in the middle, because of a lack of a direct link between them. For this packet exchange, the traditional scheduling (TS) based on point-to-point transmissions requires four time slots, while PNC requires only two time slots [1], as illustrated below

- The uplink phase of PNC (time slot 1): the two end nodes A and B send their packets X_A and X_B to the relay R simultaneously.
- The downlink phase of PNC (time slot 2): from the received overlapped signals of nodes A and B, relay R first performs XOR decoding, i.e., *decodes* a network-coded packet $X_R = X_A \oplus X_B$ using XOR, and then broadcasts X_R back to nodes A and B.

Node A (B) then decodes its desired packet X_B (X_A) from the received packet X_R and its previously transmitted packet

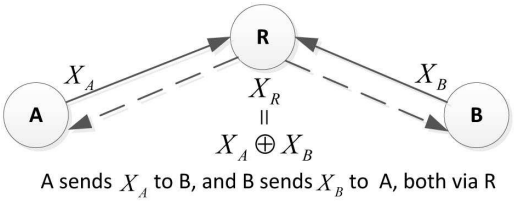

FIGURE 1. Two-way relay channel: a typical scenario for PNC to be applied.

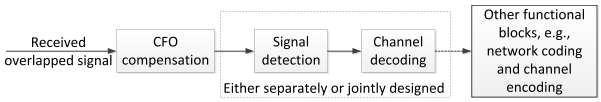

FIGURE 2. Functional blocks for relay R in PNC to deal with the CFO problem.

X_A (X_B) using $X_R \oplus X_A$ ($X_R \oplus X_B$). This way, PNC, compared with TS, halves the transmission times and thereby doubles the overall throughput of TWRC.

Signal synchronization is critical in PNC [2], [3]. In the synchronized case, the signals from the two end nodes are received aligned at relay R, i.e., with the same arriving time, phase, and frequency. In case of signal misalignment, performance penalty in PNC usually occurs [2]. Orthogonal frequency division multiplexing (OFDM) modulation could ease this synchronization problem of PNC, that is, with a sufficiently long cyclic prefix (CP), the symbol (or the arriving time) misalignment could be resolved, even in the multipath environments [4]. Therefore, OFDM modulated PNC has become a hot topic in PNC studies, e.g., it has been studied in 802.11p vehicular ad-hoc networks (VANETs) [5], [6] and in underwater acoustic communications [7].

One big challenge for OFDM modulated PNC is the carrier frequency offset (CFO) problem. CFO is caused by either node motion or local oscillator (LO) asynchrony. The node motion introduces Doppler shift to the carrier frequency of a transmit signal. This frequency shift increases with the relative velocity between the signal transmitter and receiver. The LO asynchrony refers to the case that the frequency generated at a receiver for signal downconversion is different from that used for signal upconversion at the transmitter. This also results in CFO. CFO could be estimated via training symbols, e.g., in the 802.11 frame [4], and it could be compensated in traditional single-user point-to-point communications. In PNC, however, as signals from the two end nodes may undergo different CFO values, it is not possible for relay R to completely eliminate the CFO of both signals [8]. CFO in OFDM will cause inter-carrier interference (ICI) between subcarriers [9], and the ICI is detrimental to bit error rate (BER) performance at a receiver [10]. In PNC, the situation is even more challenging, as all subcarriers from both end nodes interfere with each other at relay R.

This paper deals with the CFO problem in PNC and aims to reduce its impact on the XOR decoding of PNC via effective signal processing at relay R in TWRC. We propose a receiver for relay R that focuses primarily on CFO compensation, signal detection, and channel decoding, as shown in Fig. 2. In fact, multiple choices arise for the design of each functional block in Fig. 2; they will be considered and studied in this paper. The following summarizes the contributions of this paper:

- First, we propose a joint signal detection and channel decoding scheme at relay R in repeat-accumulate (RA) coded PNC. In this scheme, a factor graph that is dictated by both the RA code and the ICI is created, and then based on it, a belief propagation (BP) algorithm is designed for joint signal detection and channel decoding of both end nodes in TWRC.
- Second, for comparison, we also propose another two low-complexity schemes that perform signal detection and channel decoding in a disjoint manner. These two schemes differ from each other in the channel decoding.
- Third, we study different CFO compensation approaches for the proposed three schemes, and find that the approach that amounts to positioning the relay's LO frequency at the middle of the received frequencies from the end nodes is BER-optimal for all the three schemes.
- Fourth, with the joint scheme, our study shows that for low to medium CFO levels, the BER of PNC is comparable to that of traditional point-to-point communications even without CFO.

The rest of this paper is organized as follows. Section II describes the related work, and Section III gives the system model of our work. The design of the three functional blocks for relay R is presented in Section IV. Then, the simulation study is given in Section V. Finally, Section VI concludes this paper.

II. RELATED WORK

Inspired by the concept of network coding [11], PNC was pioneered in [1] in 2006, and since then, it has developed quickly into a subfield of network coding, drawing tremendous research attention in the past decade. For PNC in relay networks, a comprehensive survey was conducted in [12], where a variety of PNC design issues were illustrated and discussed. Recent studies even show that PNC is also useful in non-relay scenarios [13], [14]. In this paper, we consider PNC in TWRC, a relay scenario, and below we discuss the issues and works closely related to our study.

The relative phase offset between the received signals of the end nodes is detrimental to PNC performance. In single-carrier PNC, the BER degradation of the XOR decoding was seen in [15] for BPSK modulation, in [16] for QAM modulation, and in [17] for QPSK modulation. In OFDM based PNC, [18] studied the joint effect of the phase offset and CFO, and showed that the BER over one OFDM frame was primarily affected by CFO. This is because CFO has a

phase-rotating effect on successive OFDM symbols and thus the phase offset evolves from one symbol to another within one OFDM frame. This will also be seen in our study (to be shown in Section V) in this paper.

The symbol misalignment is a critical issue in PNC, as it introduces inter-symbol interference (ISI) at relay R. Reference [2] showed that the SINR penalty from the ISI was within 3 dB in single-carrier PNC. By contrast, [19] exploited the ISI and proposed to use BP in the signal detection of QPSK modulation, resulting in a remarkable BER performance improvement even with relative phase offset in PNC. For OFDM based PNC in the frequency domain, if the cyclic prefix (CP) is sufficiently long (or longer than the delay spread of the PNC system [4]), then there is no ISI between OFDM symbols and any time-domain symbol offset is translated into a phase offset for the frequency-domain symbols [4]. This paper assumes a relatively long CP, and thus the symbol offset is not an issue in our study.

CFO poses a big challenge for OFDM based PNC, as it destroys the orthogonality between subcarriers and thereby induces ICI. To deal with the ICI at relay R, [18] exploited the ICI structure for the signal detection in unchannel-coded PNC, and [7], [8], [20] explored iterative signal detection/decoding schemes in channel-coded PNC. In this paper, we consider both a separate and a joint design of signal detection and channel decoding to address the CFO/ICI problem in channel-coded PNC. Moreover, we study different CFO compensation approaches and seek an optimal one to match up with our proposed signal detection and channel decoding schemes.

Channel estimation is critical in PNC. For single-carrier PNC, [21] proposed a framework for joint channel estimation and decoding using both user data and pilots. For OFDM based PNC, [4] restructured the standard 802.11 frame to separate both the training symbols and the frequency-domain pilots of the end nodes. Then, relay R could use conventional estimation methods (e.g., in [23]) to simultaneously keep track of the channel gain functions and the CFO values of the two uplinks in PNC.

III. SYSTEM MODEL

This paper considers OFDM modulated PNC in a TWRC where two end nodes A and B want to exchange packets X_A and X_B via a relay R, as shown in Fig. 1. In particular, signals transmitted over every point-to-point link in Fig. 1 undergo carrier frequency offset (CFO). In the following, the details of our system model are illustrated.

The packets to be sent by nodes A and B are source bit sequences and represented as $X_A = (x_A[m])_{m=0,\ldots,M-1}$ and $X_B = (x_B[m])_{m=0,\ldots,M-1}$, respectively. Before sending their packets out, nodes A and B channel-code them, i.e., $U_A = \boldsymbol{C}(X_A) = (u_A[n])_{n=0,\ldots,N-1}$ and $U_B = \boldsymbol{C}(X_B) = (u_B[n])_{n=0,\ldots,N-1}$. Here, we assume the same linear channel code $\boldsymbol{C}(\cdot)$ used by nodes A and B. U_A and U_B are then divided into L groups to be loaded onto L OFDM symbols. We consider BPSK to map U_i to $S_i = (s_i[n])_{n=0,\ldots,N-1}$, i.e., $u_i[n] = 0$ mapped to $s_i[n] = +1$ and $u_i[n] = 1$ mapped to $s_i[n] = -1$, $i \in \{A, B\}$, and then use S_i to modulate OFDM subcarriers. For OFDM modulation, let the number of subcarriers be K, the symbol duration be T_s, and the cyclic prefix (CP) length be T_g. Then the baseband OFDM signal $s_i(t)$ transmitted by node i for $-T_g < t \le L(T_s + T_g) - T_g$ is

$$s_i(t) = \frac{1}{\sqrt{T_s}} \sum_{l=0}^{L-1} \sum_{k=0}^{K-1} \left\{ s_{i,l}[k] \cdot e^{j2\pi k \Delta_f (t - lT)} \cdot \mathrm{rect}\left(\frac{2(t - lT) + T_g - T_s}{2T} \right) \right\}, \quad (1)$$

where $\Delta_f = \frac{1}{T_s}$ is the subcarrier spacing, $s_{i,l}[k] = \pm 1$ is the k-th BPSK symbol in the l-th group of S_i, $T = T_s + T_g$ is the total symbol duration, and rect$(\cdot)$ is the rectangular pulse shaping function.

Note that pilot insertion is not considered in our model, but it does not affect the design of our signal detection and channel decoding schemes in PNC in principle, as will be discussed in Section IV. Also, note that the extension of our work to higher-order modulations, e.g., QPSK, is straightforward, as will be seen in Section IV.

We consider both the flat fading channel and the frequency-selective channel in TWRC, and as mentioned earlier, we assume the use of a sufficiently long CP to guarantee the OFDM symbols from the end nodes aligned at relay R in the frequency domain under both channel models [4]. Furthermore, we assume that power control is adopted at the end nodes so that the received power levels for X_A and X_B at relay R are balanced, as elaborated below.

A. POWER CONTROL IN PNC

For the k-th subcarrier from node i to relay R, we denote its channel gain at time t by $\gamma_{k,i}(t)$. Over the two phases of PNC, we assume the magnitude, $\|\gamma_{k,i}(t)\|$, of $\gamma_{k,i}(t)$ stays constant whereas its phase $\phi_{k,i}(t)$ may vary. Obviously, this assumption holds in static scenarios, and also in mobile scenarios like 802.11p VANETs [18] where the relative movement between node i and relay R within the two phases of PNC is only several wavelengths. Employing the special OFDM frame design in [4] at the end nodes, relay R in PNC can keep track of $\gamma_{k,A}(t)$ and $\gamma_{k,B}(t)$ at the same time. Then, through channel state information (CSI) feedback from relay R, node i can obtain $\|\gamma_{k,i}(t)\|$. Thus, in this paper we consider the following power control scheme:

$$p_i(t) = \frac{1}{\sqrt{T_s}} \sum_{l=0}^{L-1} \sum_{k=0}^{K-1} \left\{ \frac{1}{\|\gamma_{k,i}(t)\|} \cdot s_{i,l}[k] \cdot e^{j2\pi k \Delta_f (t - lT)} \cdot \mathrm{rect}\left(\frac{2(t - lT) + T_g - T_s}{2T} \right) \right\} \quad (2)$$

We have the following remarks regarding our power control scheme. First, it is analogous to the channel inversion based power control in [26] except that it does not attempt to pre-code the phase $\phi_{k,i}(t)$. Second, it becomes much less demanding in flat fading channels, as $\|\gamma_{k,i}(t)\|$ keeps the

same for all k and the power amplification can be performed on the signal $s_i(t)$ in (1) rather than on each individual subcarrier in (2). Third, it fits scenarios where a line of sight (LOS) between node i and relay R exists. This is because the deep fading problem at some subcarriers, a big challenge to our power control in the frequency-selective channel, may not be a major concern in those scenarios. Fourth, if needed, the subcarrier suppression method [26] could be integrated into our power control to effectively cope with the deep fading problem. We emphasize that with this method, the design of our signal detection and channel decoding schemes in Section IV remains the same in principle. We leave the study of the subcarrier suppression as future work.

B. PNC UNDER THE FLAT FADING CHANNEL

Consider a flat fading channel from node i to relay R. For such a channel, the multipath channel gain has only one tap and all the subcarriers have the same channel gain function, denoted by $\gamma_i(t)$. With the above power control, the signal from node i, after passing through the channel, becomes

$$\widetilde{s}_i(t) = \gamma_i(t)\, p_i(t) = e^{j\phi_i(t)}\, s_i(t) \tag{3}$$

where $\phi_i(t)$ is the phase of $\gamma_i(t)$.

Now let us first look at the received signal at relay R in PNC in static scenarios without CFO. As the signals $\widetilde{s}_A(t)$ and $\widetilde{s}_B(t)$ keep aligned, the received overlapped baseband signal $y_R(t)$ at relay R is given by

$$y_R(t) = e^{j\phi_A} s_A(t) + e^{j\phi_B} s_B(t) + n(t) \tag{4}$$

where $n(t)$ is the white Gaussian noise with zero mean and variance σ^2. Note in (4) that in static environments without CFO, $\phi_i(t)$ is a constant value equal to $\phi_i(0) = \phi_i$. Then, at relay R, the received signal $y_R(t)$ is multiplied with a bank of K correlators and integrated over the period $\left[l(T_s+T_g), l(T_s+T_g)+T_s\right)$ for the l-th OFDM symbol, $0 \le l \le L-1$. In the following, without loss of generality, let us look at the correlator output for the first OFDM symbol, and to simplify the notations, we use $s_{i,0}[k] = s_i[k]$. Then, the output at the m-th correlator ($0 \le m \le K-1$) is

$$y_R[m] = \frac{1}{\sqrt{T_s}} \int_0^{T_s} y_R(t) e^{-j2\pi m \Delta_f t} dt \tag{5}$$

Without CFO, it can be seen from (5) that only information $s_A[m]$ and $s_B[m]$ sent through subcarrier m from both end nodes will be present at the m-th correlator output, and information carried by other subcarriers $k \neq m$ will be eliminated. We consider PNC in the frequency domain based on OFDM, and the ultimate goal of relay R is to channel-decode $X_R = (x_A[m] \oplus x_B[m])_{m=0,\ldots,M-1}$ (i.e., perform the XOR decoding of X_R) from the correlator output of all OFDM symbols and then use the same channel code as used at the end nodes to encode X_R, i.e., $U_R = \boldsymbol{C}(X_R)$, before broadcasting X_R back to the end nodes. In the situation of (5), Section IV will show that the decoding of X_R is greatly simplified.

CFO, however, will induce inter-carrier interference (ICI) among subcarriers. CFO occurs when there is a mismatch between relay R's LO frequency and the carrier frequency of the received signal. Node motion and/or local oscillator (LO) asynchrony could cause this mismatch. Let the relative velocity between node i and relay R be v_i and the LO frequency of node i (relay R) for signal upconversion (downconversion) be $f_{o,i}$ ($f_{o,R}$). Then, the overall CFO, f_{δ_i}, of the link from node i to relay R is approximately given by $f_{d,i} + f_{o,i} - f_{o,R}$ [27], where $f_{d,i}$ is the Doppler shift given by

$$f_{d,i} = \frac{v_i}{c} f_{o,i} \tag{6}$$

where c is the speed of waves (e.g., EM waves, sound waves, etc.). Note that f_{δ_i} can be estimated by relay R, e.g., using training symbols [4]. Here, we define the normalized CFO of the link from node i to relay R as $\delta_i = f_{\delta_i}/\Delta_f$. With CFO considered, the overlapped signal $y_R(t)$ becomes

$$y_R(t) = s_A(t)\, e^{j(2\pi f_{\delta_A} t + \phi_A)} + s_B(t)\, e^{j(2\pi f_{\delta_B} t + \phi_B)} + n(t) \tag{7}$$

Note in (7) that a narrowband TWRC or a much higher carrier frequency $f_{c,i}$ relative to the bandwidth of $s_i(t)$ is assumed such that all subcarriers of node i undergo the same Doppler shift $f_{d,i}$. Substituting (1) and (7) into (5), we have

$$y_R[m] = \sum_{i\in\{A,B\}} \left\{ \frac{e^{j\phi_i}}{T_s} \times \sum\nolimits_k \int_0^{T_s} s_i[k] e^{j2\pi(k-m+\delta_i)\Delta_f t}\, dt \right\} + w_m \tag{8}$$

where $w_m = \frac{1}{\sqrt{T_s}} \int_0^{T_s} n(t) e^{-j2\pi m \Delta_f t} dt$ is the noise at the m-th correlator. It can be found that the variance of w_m remains σ^2. Put $u = m - k$, and let

$$\begin{aligned} a_{u,i} &= \frac{1}{T_s} \int_0^{T_s} e^{-j2\pi(u-\delta_i)\Delta_f t} dt \\ &= \mathrm{sinc}(u-\delta_i)\, e^{-j\pi(u-\delta_i)} \end{aligned} \tag{9}$$

where $\mathrm{sinc}(x) = \frac{\sin(\pi x)}{\pi x}$. Here, $a_{u,i} \neq 0$, for $u \neq 0$ or $k \neq m$, represents the generation of the ICI from the k-th subcarrier on the m-th subcarrier. In this paper, we assume $-0.5 \le \delta_i \le 0.5$. This usually holds in scenarios where LO has high stabilities [28] and Doppler shift is limited relative to the subcarrier spacing Δ_f [5]. VANETs are such scenarios as shown in [18]. With this scope of δ_i, it is not difficult to see that among all $\|a_{u,i}\|^2$, $u \neq 0$, the largest is either $\|a_{1,i}\|^2$ or $\|a_{-1,i}\|^2$, depending on the sign of δ_i. Substituting (9) into (8), we have

$$\begin{aligned} y_R[m] &= \sum_{i\in\{A,B\}} e^{j\phi_i} \sum_{u=m-K+1}^{m} a_{u,i} s_i[m-u] + w_m \\ &= \underbrace{\sum_{i\in\{A,B\}} e^{j\phi_i} a_{0,i} s_i[m]}_{\text{desiredsignal}} \\ &\quad + \underbrace{\sum_{i\in\{A,B\}} \sum_{u\neq 0} e^{j\phi_i} a_{u,i} s_i[m-u]}_{\text{PNC\_ICI}} + \underbrace{w_m}_{\text{noise}} \end{aligned} \tag{10}$$

where the first term on the RHS is the desired signal at the m-th correlator output, and the second term corresponds to the overall ICI for the m-th subcarrier in the PNC uplink phase. From (10), we see that the relative phase offset between the desired signals of nodes A and B is given by $\Delta\theta = \phi_A - \phi_B + \pi(\delta_A - \delta_B)$, which applies to every subcarrier in the first OFDM symbol over time $[0, T_s]$. Indeed, the relative phase offset for the l-th symbol evolves into $\Delta\theta(l) = \phi_A - \phi_B + \pi(\delta_A - \delta_B) + 2\pi l(\delta_A - \delta_B)(T_s + T_g)/T_s, 0 \le l \le L-1$. Hence, we see that CFO has a phase-rotating effect on successive OFDM symbols.

Similarly, for the traditional scheduling (TS) based on point-to-point communications, the received signal, $y_i(t)$, from node i at relay R is

$$y_i(t) = s_i(t)\, e^{j(2\pi f_{\delta_i} t + \phi_i)} + n(t) \tag{11}$$

and after integration, the m-th correlator output is given by

$$y_i[m] = \underbrace{e^{j\phi_i} a_{0,i} s_i[m]}_{\text{desiredsignal}} + \underbrace{\sum\nolimits_{u\neq 0} e^{j\phi_i} a_{u,i} s_i[m-u]}_{\text{ICI}} + \underbrace{w_m}_{\text{noise}} \tag{12}$$

From (10) and (12), we see that PNC suffers from more intense ICI than TS. With the joint design of signal detection and channel decoding at relay R, however, we will show that the BER performance of PNC is comparable to that of TS.

C. PNC UNDER THE FREQUENCY-SELECTIVE CHANNEL

Now assume a frequency-selective channel from node i to relay R. For such a channel, the multipath gain has multiple taps, and each tap is associated with a channel gain and a time delay. The delay spread of the channel is defined as the maximal difference between these time delays. This paper assumes that the delay spread of each channel in TWRC is no more than the CP length T_g, yielding a flat fading for each subcarrier but different channel gains for different subcarriers [4]. We use $\gamma_{k,i}(t)$ for the channel gain of the k-th subcarrier from node i. With the power control applied to each individual subcarrier at node i, we have the m-th correlator output for the first OFDM symbol in PNC given by

$$\begin{aligned} y_R[m] = &\sum_{i\in\{A,B\}} e^{j\phi_{m,i}} a_{0,i} s_i[m] \\ &+ \sum_{i\in\{A,B\}} \sum_{u\neq 0} e^{j\phi_{m-u,i}} a_{u,i} s_i[m-u] + w_m \end{aligned} \tag{13}$$

Similarly, the m-th correlator output in TS is given by

$$y_i[m] = e^{j\phi_{m,i}} a_{0,i} s_i[m] + \sum_{u\neq 0} e^{j\phi_{m-u,i}} a_{u,i} s_i[m-u] + w_m, \tag{14}$$

In both (13) and (14), $\phi_{m,i}$ is the phase of $\gamma_{m,i}(t)$ at $t = 0$.

IV. RECEIVER DESIGN FOR RELAY R IN PNC

In this section, we present the receiver design of the relay in PNC to deal with the CFO problem in (10), i.e, in the flat fading channel. It encompasses CFO compensation, signal detection, and channel decoding at relay R, i.e., the design of the three functional blocks shown in Fig. 2. Particularly, for the latter two blocks, we consider both a separate design and a joint design. We assume in the design that the channel parameters ϕ_i and δ_i for $i \in \{A, B\}$ are already known to relay R through channel estimation [4]. Note that the receiver design under the frequency-selective channel is similar, as will be discussed later in this section.

A. DESIGN OF CFO COMPENSATION

This block processes the downconverted OFDM signal of (7). Using signal processing techniques, e.g., via sampling the signal of (7), relay R could adjust the CFO values f_{δ_A} and f_{δ_B} in (7) simultaneously, which is equivalent to adjusting relay R's LO frequency $f_{o,R}$ in the signal downconversion. Let us assume relay R's LO frequency is shifted to $f_{o,R} + \tau$. In the literature, three CFO compensation approaches have been proposed [4], [8], [18], each corresponding to one choice of choosing τ. The first approach is to choose $\tau = f_{\delta_A}$ to completely eliminate the CFO from node A, and similarly, the second chooses $\tau = f_{\delta_B}$ to eliminate the CFO from node B. Both approaches, however, leave behind the other CFO value. The third approach, named mean-valued (MV) CFO compensation in [18], sets $\tau = \frac{f_{\delta_A} + f_{\delta_B}}{2}$, leaving the CFO values from the two end nodes opposite to each other, equal to $\frac{f_{\delta_A} - f_{\delta_B}}{2}$ and $\frac{f_{\delta_B} - f_{\delta_A}}{2}$, respectively. In our study, we consider not just these three choices of τ, but many more (to be shown in the next section). However, our study will show that the MV compensation approach is optimal for all the three signal detection and channel decoding schemes to be presented below. Note that when $f_{o,R}$ is shifted to $f_{o,R} + \tau$, f_{δ_A} and f_{δ_B} in (7) are replaced with $f_{\delta_A} - \tau$ and $f_{\delta_B} - \tau$, respectively.

B. DESIGN OF SIGNAL DETECTION AND CHANNEL DECODING

These two blocks are built based on the correlator output at relay R, and the ultimate goal of them is to find the XORed source bit sequence $X_R = X_A \oplus X_B = (x_A[m] \oplus x_B[m])_{m=0,\ldots,M-1}$. In our design, the signal detector is to find the *a posteriori* probabilities (APP) of the channel-coded bit pair $(u_A[n], u_B[n])$, $0 \le n \le N-1$, given all the correlator ouput $y_{R,l}[k]$ (i.e., the k-th correlator output of the l-th OFDM symbol in PNC, $0 \le k \le K-1$ and $0 \le l \le L-1$), and the channel decoder is to perform channel decoding $\boldsymbol{C}^{-1}(\cdot)$ to find X_R eventually. This paper assumes the use of repeat-accumulate (RA) code in the TWRC system [19], [22]. RA code is a competitive alternative to turbo code and low-density parity-check (LDPC) code, and it has a low encoding complexity [22]. There are multiple ways to connect these two blocks. The following are the three schemes of the connections to be considered in this paper:

- Scheme 1: This scheme performs joint signal detection and channel decoding. It takes all the correlator output $y_{R,l}[k]$ as input to compute the APP $\Pr(x_A[m], x_B[m]|y_{R,l}[k]\forall l, k)$ for any m and then to produce X_R. $\Pr(x_A[m], x_B[m]|y_{R,l}[k]\forall l, k)$ is computed from the APP $\Pr(X_A, X_B|y_{R,l}[k]\forall l, k)$ through marginalization. For the latter APP, a factorization that is dictated by the ICI and the channel code $\boldsymbol{C}(\cdot)$ is considered. Based on that factorization, a belief propagation (BP) algorithm is then designed to compute the former APP.
- Scheme 2: This scheme (and the next scheme) adopts a separate design of signal detection and channel decoding. The signal detector first finds the APP $\Pr(u_A[n], u_B[n]|y_{R,l}[k]\forall l, k)$ and then feeds them into the channel decoder, where channel decoding is performed on the vector sequence $(u_A[n], u_B[n])_{n=0,\ldots,N-1}$. In particular, this channel decoder aims to first compute the soft information $\Pr(x_A[m], x_B[m])$ and then output the XORed sequence X_R.
- Scheme 3: The signal detector here first finds $\Pr(u_A[n]\oplus u_B[n]|y_{R,l}[m]\forall l, m)$ and then feeds them into the channel decoder, where $X_R = \boldsymbol{C}^{-1}(U_A \oplus U_B)$ is performed. Note that due to the linearity of the channel code $\boldsymbol{C}(\cdot)$, we have $X_R = X_A \oplus X_B = \boldsymbol{C}^{-1}(U_A) \oplus \boldsymbol{C}^{-1}(U_B) = \boldsymbol{C}^{-1}(U_A \oplus U_B)$. This scheme shares the same principle of design as the XOR-CD model in [19].

In the following, we present the frameworks for the three schemes above in detail based on RA code. Note that the frameworks for other channel codes (e.g., turbo and LDPC codes) that use BP for decoding can be similarly designed.

Scheme 1: The APP $\Pr(X_A, X_B|y_{R,l}[k]\forall l, k)$ satisfies:

$$\begin{aligned}&\Pr(X_A, X_B|y_{R,l}[k]\forall l, k)\\ &\propto \Pr(y_{R,l}[k]\forall l, k|(X_A, X_B))\\ &= \Pr(U_A, U_B, y_{R,l}[k]\forall l, k|(X_A, X_B)) \cdot \boldsymbol{\Lambda}(X_A, X_B, U_A, U_B)\\ &= \Pr(y_{R,l}[k]\forall l, k|(U_A, U_B)) \cdot \boldsymbol{\Lambda}(X_A, X_B, U_A, U_B), \qquad (15)\end{aligned}$$

where $\boldsymbol{\Lambda}(\cdot)$ is an indicator function that introduces constraints on both (U_A, X_A) and (U_B, X_B) from the channel code $\boldsymbol{C}(\cdot)$ and is given by

$$\begin{aligned}&\boldsymbol{\Lambda}(X_A, X_B, U_A, U_B)\\ &\quad= \begin{cases}1, & \text{if } (U_A, U_B) = (\boldsymbol{C}(X_A), \boldsymbol{C}(X_B)),\\ 0, & \text{otherwise}.\end{cases} \qquad (16)\end{aligned}$$

With RA code, $\boldsymbol{\Lambda}(\cdot)$ can be factorized into a series of indicator functions, each corresponding to a local constraint from the encoding process of $\boldsymbol{C}(X_A)$ and $\boldsymbol{C}(X_B)$. Fig. 3 depicts $\boldsymbol{C}(X_A)$ and $\boldsymbol{C}(X_B)$, encompassing bit repeating (with repeat factor $q = \frac{N}{M}$), interleaving, and accumulating [19], and given by the the blue circles are the constraints/factors pertaining to this process (more details on these factors are given below).

We have the following two observations to expand $\Pr(y_{R,l}[k]\forall l, k|(U_A, U_B))$ in (15). First, as we assume a long CP in OFDM, there is no inter-symbol-interference (ISI) in the uplink transmission of PNC. Hence, for a given l, all

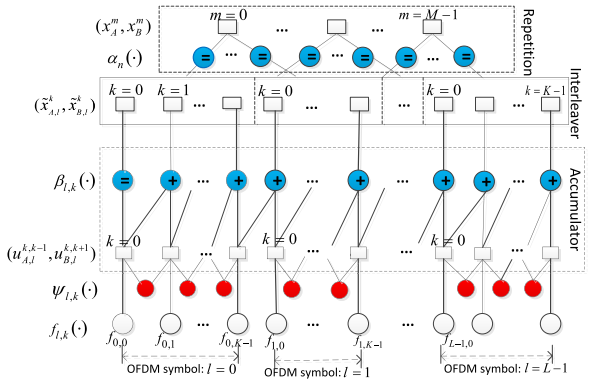

FIGURE 3. A factor graph for signal detection and channel decoding in Scheme 1.

$y_{R,l}[k]$ depend only on the l-th OFDM symbol, thus resulting in the following expansion:

$$\Pr(y_{R,l}[k]\forall l, k|(U_A, U_B)) = \prod_{l=0}^{L-1} \Pr(y_{R,l}[k]\forall k|(U_{A,l}, U_{B,l})) \qquad (17)$$

where $U_{i,l} = (u_{i,l}[k])_{k=0,\ldots,K-1}$ denotes the coded bit sequence in the l-th OFDM symbol of node i. Second, for the first OFDM symbol, we see from (10) that any of its coded bit pairs $(u_A[n], u_B[n])$ $(0 \le n \le K-1)$ is involved in all of its correlator output, acting as either the desired signal or the ICI. Importantly, for the k-th correlator output $y_R[k]$ in (10), [18] showed that the subcarriers from node i that contributed most power to $y_R[k]$ were the k-th and $k-1$-th (the k-th and $k+1$-th) subcarriers when $0 \le \delta_i < 0.5$ (when $-0.5 < \delta_i < 0$). This applies to the correlator output of any OFDM symbol indeed. Thus, as in [18], it is also deemed in this paper that *each correlator output is composed of only those power-dominating subcarriers as well as the noise*. Consequently, each term in (17) can be further factorized, and the factorization is divided into the following four cases: (a) $\delta_A \ge 0$ and $\delta_B \ge 0$; (b) $\delta_A \ge 0$ and $\delta_B < 0$; (c) $\delta_A < 0$ and $\delta_B \ge 0$; and (d) $\delta_A < 0$ and $\delta_B < 0$. The following factorizes the l-th term:

$$\begin{aligned}&\Pr(y_{R,l}^k\forall k|(U_{A,l}, U_{B,l}))\\ &= \begin{cases}\prod_{k=0}^{K-1} \Pr(y_{R,l}^k|(u_{A,l}^{k,k-1}, u_{B,l}^{k,k-1})), & \text{for case } (a);\\ \prod_{k=0}^{K-1} \underbrace{\Pr(y_{R,l}^k|(u_{A,l}^{k,k-1}, u_{B,l}^{k,k+1}))}_{=f_{l,k}(u_{A,l}^{k,k-1}, u_{B,l}^{k,k+1})}, & \text{for case } (b);\\ \prod_{k=0}^{K-1} \Pr(y_{R,l}^k|(u_{A,l}^{k,k+1}, u_{B,l}^{k,k-1})), & \text{for case } (c);\\ \prod_{k=0}^{K-1} \Pr(y_{R,l}^k|(u_{A,l}^{k,k+1}, u_{B,l}^{k,k+1})), & \text{for case } (d);\end{cases} \qquad (18)\end{aligned}$$

Note in (18) and below that we use $y_{R,l}^k = y_{R,l}[k]$, $u_{i,l}^k = u_{i,l}[k]$, and $u_{i,l}^{m,n} = (u_{i,l}[m], u_{i,l}[n])$, and that $u_{i,l}^{-1}$ and $u_{i,l}^K$, arising when $k=0$ and $k=K$ respectively, are imaginary bits that have nothing to do with the probability evaluation.

The factorization of $\Pr(X_A, X_B|y_{R,l}^k\forall l, k)$ above can be visualized as a factor graph [24]. Fig. 3 is such a factor

TABLE 1. Message types in the factor graph of Fig. 3.

Message type	Interpretation	Message type	Interpretation
$D_1^{m,n}(\cdot)$	Message from (x_A^m, x_B^m) to α_n	$U_1^{m,n}(\cdot)$	Message from α_m to (x_A^n, x_B^n)
$D_2^{m,n}(\cdot)$	Message from α_m to $\tilde{X}_n$	$U_2^{m,n}(\cdot)$	Message from $\tilde{X}_m$ to α_n
$D_3^{m,n}(\cdot)$	Message from $\tilde{X}_m$ to β_n	$U_3^{m,n}(\cdot)$	Message from β_m to $\tilde{X}_n$
$D_4^{m,n}(\cdot)$	Message from β_m to $\tilde{U}_n$	$U_4^{m,n}(\cdot)$	Message from $\tilde{U}_m$ to β_n
$M_1^{m,n}(\cdot)$	Message from $\tilde{U}_m$ to ψ_n	$M_2^{m,n}(\cdot)$	Message from ψ_m to $\tilde{U}_n$
$U_5^{m,m}(\cdot)$	Message from f_m to $\tilde{U}_m$	–	

graph in case (b), where squares (called variable nodes) are bit vectors and circles (called check nodes) represent constraints on the connected bit vectors. $\alpha_n(\cdot)$ is used to guarantee the two bit vectors connected to it are identical, and $\beta_{l,k}(\cdot)$ is defined such that (i) for $k \neq 0$, $u_{i,l}^{k-1} \oplus \tilde{x}_{i,l}^k = u_{i,l}^k$, $i \in \{A, B\}$; (ii) for $l = 0$ and $k = 0$, $\tilde{x}_{i,l}^k = u_{i,l}^k$; and (iii) for $l > 0$ and $k = 0$, $u_{i,l-1}^{K-1} \oplus \tilde{x}_{i,l}^k = u_{i,l}^k$. Each bit above is from only one variable node connected to $\beta_{l,k}(\cdot)$. One possible definition of $\beta_{l,k}(\cdot)$ is considered in the appendix. Particularly, the red circles $\psi_{l,k}(\cdot)$ are indicator functions that come as additional factors/constraints to ensure that any common coded bit between $(u_{A,l}^{k,k-1}, u_{B,l}^{k,k+1})$ and $(u_{A,l}^{k+1,k}, u_{B,l}^{k+1,k+2})$ takes on the same value. Factor graphs in the other three cases can be similarly drawn.

With a factor graph for $\Pr(X_A, X_B | y_{R,l}^k \forall l, k)$, a BP algorithm can be designed to facilitate the computation of $\Pr(x_A^m, x_B^m | y_{R,l}^k \forall l, k)$. BP employs message passing for probability marginalization. Here, we focus on the message passing in Fig. 3, as the situations in the other three cases are similar. For the sake of presentation below, we first renumber the variable nodes and the check nodes as follows: $f_{l,k}(\cdot) = f_{l\cdot K+k}(\cdot)$, $\phi_{l,k}(\cdot) = \phi_{l\cdot K+k}(\cdot)$, $\beta_{l,k}(\cdot) = \beta_{l\cdot K+k}(\cdot)$, $(\tilde{x}_{A,l}^k, \tilde{x}_{B,l}^k) = \tilde{X}_{l\cdot K+k}$, and $(u_{A,l}^{k,k-1}, u_{B,l}^{k,k+1}) = \tilde{U}_{l\cdot K+k}$. Then Table 1 defines the message types from top to bottom in Fig. 3.

Note that messages apply only between two connected nodes in Fig. 3. A message either entering or emanating from a variable node informs the receiver node of *the probability distribution of the bit vector of the variable node*. In BP, if an incoming message of a node is updated, then its outgoing messages to other connected nodes will also be updated. The update process is guided by message passing/update rules, which specify not only the sequence of updating messages but also how each message is updated. The update rules for Fig. 3 are summarized as follows, and the details are included in Appendix.

Step 1 (Initializing Messages):. Any message in Table 1 but $U_5^{m,m}$ is initialized with equal probabilities for the bit vector it is associated with. $U_5^{m,m}$, the message flowing from f_m to $\tilde{U}_m$, is equal to f_m. For a given $m = l \cdot K + k$, we define the following distance function with respect to $y_{R,l}^k$

$$d(u_A^{m,m-1}, u_B^{m,m+1}) = \left\| y_{R,l}^k - e^{j\theta_{A,l}}(a_{0,A}s_A^m + a_{1,A}s_A^{m-1}) - e^{j\theta_{B,l}}(a_{0,B}s_B^m + a_{-1,B}s_B^{m+1}) \right\|, \quad (19)$$

where $\theta_{i,l} = \phi_i + 2\pi f_{\delta_i} l(T_s + T_g)$ is a phase term related to the l-th OFDM symbol, and $s_i^m = 1 - u_i^m$ is a BPSK symbol. In case that $k = 0$ ($k = K - 1$), the term with s_A^{m-1} (s_B^{m+1}) will not appear in (19). Then, we have

$$U_5^{m,m}(u_A^{m,m-1}, u_B^{m,m+1}) \propto \exp\{-\frac{d^2(u_A^{m,m-1}, u_B^{m,m+1})}{\sigma^2}\}. \quad (20)$$

Step 2 (Updating $M_1^{m,n}(\cdot)$ and $M_2^{m,n}(\cdot)$): This step updates messages between $\tilde{U}_m$ and ψ_m within each OFDM symbol, as shown in Fig. 3. The update rules keep the same for messages within every symbol. The messages $M_1^{m,n}$ and $M_2^{m,n}$ in Fig. 3 are updated from left to right and from right to left. For symbol $l = 0$, for example, the update sequences in these two directions are $\{M_1^{0,0}\ M_2^{0,1}\ \ldots\ M_1^{k,k}\ M_2^{k,k+1}\ M_1^{k+1,k+1}\ \ldots\ M_2^{K-2,K-1}\}$ and $\{M_1^{K-1,K-2}\ M_2^{K-2,K-2}\ \ldots\ M_1^{k,k-1}\ M_2^{k-1,k-1}\ M_1^{k-1,k-2}\ \ldots M_2^{0,0}\}$, respectively. A message emanating from a node is updated using the incoming messages of that node; see details in Appendix.

Step 3 (Updating $U_4^{m,n}(\cdot)$): For any variable node $\tilde{U}_m$, its outgoing messages $U_4^{m,m}$ to β_m and $U_4^{m,m+1}$ to β_{m+1} (if any) are to be updated simultaneously in this step. See Appendix for how the two new messages are composed using the incoming messages of $\tilde{U}_m$.

Step 4 (Updating $U_3^{m,n}(\cdot)$): $U_3^{m,n}$ is updated using $U_4^{m,n}$ in step 3. For $m = 0$, $U_3^{0,0}$ is updated using $U_4^{0,0}$, and for $m > 0$, $U_3^{m,m}$ is updated using $U_4^{m-1,m}$ and $U_4^{m,m}$. See details in the appendix.

Step 5 (Updating $U_2^{m,n}(\cdot)$ and $U_1^{m,n}(\cdot)$): Suppose the variable node $\tilde{X}_m$ is connected to the factor node α_n, then $U_2^{m,n}$ is equal to $U_3^{m,m}$ in step 4. As α_n is only connected to $(x_A^{\lfloor n/q \rfloor}, x_B^{\lfloor n/q \rfloor})$, $U_1^{n,\lfloor n/q \rfloor}$ is updated and equal to $U_2^{m,n}$.

Step 6 (Updating $D_1^{m,n}(\cdot)$, $D_2^{m,n}(\cdot)$, and $D_3^{m,n}(\cdot)$): The outgoing message $D_1^{m,n}$ from (x_A^m, x_B^m) to α_n is updated using the product of the incoming messages $U_1^{k,m}$ in step 5, with $m \cdot q \leq k \leq (m+1) \cdot q - 1$ and $k \neq n$. Suppose α_n is connected to $\tilde{X}_j$, then we have $D_2^{n,j} = D_3^{j,j} = D_1^{m,n}$.

Step 7 (Updating $D_4^{m,n}(\cdot)$): With the updated $D_3^{m,m}$ in step 6, $D_4^{m,m}$ to $\tilde{U}_m$ and $D_4^{m,m-1}$ to $\tilde{U}_{m-1}$ (if any) are to be updated here. $D_4^{m,m}$ is updated using $D_3^{m,m}$ and $U_4^{m-1,m}$ (if any), and $D_4^{m,m-1}$ is updated using $D_3^{m,m}$ and $U_4^{m,m}$. See details in the appendix.

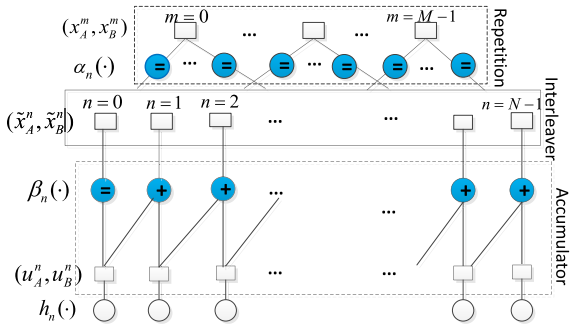

FIGURE 4. A factor graph for channel decoding in Scheme 2.

An iterative message passing is needed in Fig. 3 due to the existence of loops in the factor graph [19], [24]. The seven steps above form the first round of message passing, and the steps from 2 to 7 are iterated in the subsequent rounds. After a number of iterations, $\Pr(x_A^m, x_B^m | y_{R,l}^k \forall l, k)$ is computed as follows [29]

$$\Pr(x_A^m, x_B^m | y_{R,l}^k \forall l, k) = \prod_{n=m\cdot q}^{(m+1)\cdot q-1} D_1^{m,n}(x_A^m, x_B^m). \quad (21)$$

Eventually, $X_R = (x_A^m \oplus x_B^m)_{m=0,\ldots,M-1}$ is decoded by finding $x_A^m \oplus x_B^m$ as follows

$$x_A^m \oplus x_B^m = \arg\max_a \sum_{(x_A^m, x_B^m): x_A^m \oplus x_B^m = a} \Pr(x_A^m, x_B^m | y_{R,l}^k \forall l, k), \quad (22)$$

where $a \in \{0, 1\}$.

Scheme 2: In this scheme, the signal detector and the channel decoder function separately and explicitly. The detector computes $\Pr(u_A^n, u_B^n | y_{R,l}^k \forall l, k)$, and then the decoder channel-decodes $(u_A^n, u_B^n)_{n=0,\ldots,N-1}$ to find $\Pr(x_A^m, x_B^m)$ and X_R.

We obtain $\Pr(u_A^n, u_B^n | y_{R,l}^k \forall l, k)$ from $\Pr(U_A, U_B | y_{R,l}^k \forall l, k)$ through marginalization. Since $\Pr(U_A, U_B | y_{R,l}^k \forall l, k) \propto \Pr(y_{R,l}{}^k \forall l, k | (U_A, U_B))$, we can factor $\Pr(U_A, U_B | y_{R,l}^k \forall l, k)$ as in (17) and (18) and visualize it using the factor graph below β_n in Fig. 3 for case (b). This subgraph captures the ICI among the subcarriers, and the message passing on it encompasses only the first two steps in **Scheme 1** above. Thanks to the tree structure of this subgraph, only one round of message passing is needed for probability convergence [24], that is, after steps 1 and 2, we have

$$\begin{aligned}&\Pr(u_A^n, u_B^n | y_{R,l}^k, \forall l, k)\\ &= \sum_{u_A^{n-1}} \sum_{u_B^{n+1}} \Big\{ f_n(u_A^{n,n-1}, u_B^{n,n+1})\\ &\quad \times M_2^{n-1,n}(u_A^{n,n-1}, u_B^{n,n+1}) \times M_2^{n,n}(u_A^{n,n-1}, u_B^{n,n+1}) \Big\}. \end{aligned} \quad (23)$$

In (23), the message $M_2^{n-1,n}$ (the message $M_2^{n,n}$) is not applicable when $n \pmod K = 0$ (when $n \pmod K = K-1$).

A factor graph for channel-decoding $(u_A^n, u_B^n)_{n=0,\ldots,N-1}$ is plotted in Fig. 4, where α_n and β_n can be defined in a manner similar to Fig. 3, and h_n is given by (23). In Fig. 4, defining the message types as in Table 1, we can iterate the steps from 3 to 7 above to design the message passing rules, of which details are omitted here. After multiple rounds of decoding, we obtain $\Pr(x_A^m, x_B^m)$ as in (21) and X_R as in (22).

Scheme 3: The detector here attempts to find $\Pr(u_A^n \oplus u_B^n | y_{R,l}^k \forall l, k)$. This is done by first computing $\Pr(u_A^n, u_B^n | y_{R,l}^k \forall l, k)$. In case (b), based on (23), we have

$$\begin{aligned}\Pr(u_A^n \oplus u_B^n = a | y_{R,l}^k \forall l, k) &= \sum_{(u_A^n, u_B^n): u_A^n \oplus u_B^n = a} \Pr(u_A^n, u_B^n | y_{R,l}^k \forall l, k) \end{aligned} \quad (24)$$

where $a \in \{0, 1\}$.

Taking (24) as input, the decoder channel-decodes $U_A \oplus U_B = (u_A^n \oplus u_B^n)_{n=0,\ldots,N-1}$ into X_R. Here, the decoder is a conventional RA decoder for point-to-point communications [19], and the factor graph shares the same structure as in Fig. 4 except that the bit vectors (x_A^m, x_B^m), $(\tilde{x}_A^n, \tilde{x}_B^n)$, and (u_A^n, u_B^n) are respectively replaced by the bit scalars $x_A^m \oplus x_B^m$, $\tilde{x}_A^n \oplus \tilde{x}_B^n$, and $u_A^n \oplus u_B^n$. Also, the message passing for finding $\Pr(x_A^m \oplus x_B^m)$ and X_R can be designed in a way similar to that in Fig. 4.

C. COMPLEXITY ANALYSIS

We now compare the complexities of the three proposed schemes. We consider case (b) for comparison, because it is the case when the optimal MV CFO compensation is applied in PNC. Here, the complexity of each scheme is in terms of the number of messages to be composed/updated in its message passing process. Let us assume the size of the modulation scheme adopted in the PNC system is N_m (e.g., $N_m = 2$ for BPSK and $N_m = 4$ for QPSK). The complexity of Scheme 1 is as follows. In step 1, the number of messages $U_5^{m,m}$ to be computed is $O(LKN_m^4)$. In step 2, according to (25), (26), (27), and (28), the complexity of the message passing in the two directions is $O(4L(K-1)N_m^4)$. Similarly, the complexity in step 3 is $O((2LK-1)N_m^4)$, and the complexity in step 4 is $O(LKN_m^2)$. Step 5 does not incur any new computation overhead. In steps 6 and 7, the complexities are $O(LKN_m^2)$ and $O((2LK-1)N_m^4)$, respectively. Therefore, as the decoding rounds $N_d \to \infty$, the overall complexity of Scheme 1 is $O((8LK-4L-2)N_dN_m^4 + 2LKN_dN_m^2)$. By the same token, we find the complexities of Schemes 2 and 3 are $O((6LK-2)N_dN_m^2)$ and $O((6LK-2)N_dN_m)$, respectively. Table 2 compares the complexities of the three schemes in detail. We see that Scheme 1 has the highest complexity, yet it is the best performer in general as will be shown in Section V.

D. DISCUSSION

Here, we discuss several issues related to the receiver design for the relay R in PNC.

First, under frequency-selective channels in TWRC, the factor graphs of the three schemes remain the same as those under the flat fading channels, and hence the three schemes can be similarly designed. However, the messages $U_5^{m,m}$ in (20) are now evaluated according to (13).

TABLE 2. Complexity comparison among the three schemes.

	Scheme 1	Scheme 2	Scheme 3
Step 1	$O(LKN_m^4)$	$O(LKN_m^4)$	$O(LKN_m^4)$
Step 2	$O(4L(K-1)N_dN_m^4)$	$O(4L(K-1)N_m^4)$	$O(4L(K-1)N_m^4)$
Step 3	$O((2LK-1)N_dN_m^4)$	$O((2LK-1)N_dN_m^2)$	$O((2LK-1)N_dN_m)$
Step 4	$O(LKN_dN_m^2)$	$O(LKN_dN_m^2)$	$O(LKN_dN_m)$
Step 5	0	0	0
Step 6	$O(LKN_dN_m^2)$	$O(LKN_dN_m^2)$	$O(LKN_dN_m)$
Step 7	$O((2LK-1)N_dN_m^4)$	$O((2LK-1)N_dN_m^2)$	$O((2LK-1)N_dN_m)$
Overall (as $N_d \to \infty$)	$O((8LK-4L-2)N_dN_m^4+2LKN_dN_m^2)$	$O((6LK-2)N_dN_m^2)$	$O((6LK-2)N_dN_m)$

Second, in case that no CFO occurs, the factor graphs for the three schemes can be simplified, and the complexity of each scheme will be reduced considerably. Referring to Fig. 3, for example, the variable nodes $(u_A^{m,m-1}, u_B^{m,m+1})$ will be replaced with (u_A^m, u_B^m), and there are no check nodes ψ_m in the factor graph, thus reducing the complexity of the message passing in Scheme 1.

Third, our frameworks of the three schemes can be extended to higher order modulations. For QPSK modulation, for example, the factor graphs of all the three schemes remain the same, except that each variable (e.g., x_i^m and u_i^m) contained in the variable nodes will double its size to take two bits to correspond to the QPSK symbols. Hence, the complexity of each scheme for a high-order modulation will increase drastically.

Fourth, our frameworks can handle pilot insertion in OFDM symbols. Consider the case that one variable in the variable nodes $(u_A^{m,m-1}, u_B^{m,m+1})$ in Fig. 3 is fixed as a pilot symbol. Then, the modifications to the factor graph include: (i) a new check node to constrain the possible values of the variable is needed, and (ii) the connections between the nodes β_n and the nodes $(u_A^{m,m-1}, u_B^{m,m+1})$ may have to be rearranged, as pilot symbols do not participate in the channel coding.

Fifth, with modifications, our frameworks can also incorporate subcarrier suppression to combat deep fading. Once a subcarrier is not used, the modifications to the factor graphs include: (i) the variable corresponding to that subcarrier should be removed; (ii) the check nodes ψ_m should be updated due to the nonexistence of the variable; (iii) the message initialization in (20) should not take the canceled variable into consideration, and (iv) new connections between β_n and coded bits/symbols, e.g., $(u_A^{m,m-1}, u_B^{m,m+1})$, may be needed.

V. SIMULATION STUDY

In this section, we present simulation studies of the BER performance of the three schemes at relay R under various conditions. The simulation settings are as follows. The packets X_A and X_B have the same length of 240 bytes, and the repeat factor q of the RA code is set 3. For the OFDM modulation, we adopt the basic settings of the IEEE 802.11p standard [25]: the 10 MHz bandwidth is divided into 64 subbands, yielding $K = 64$ subcarriers in one OFDM symbol and $T_s = 6.4$ μs for the symbol duration, and the CP length is set to be $T_g = \frac{T_s}{4} = 1.6$ μs. All the 64 subcarriers are used as data subcarriers in our study. Thus, after channel coding, each packet to be sent out is composed of $L = 90$ OFDM symbols. In the following, the first three studies assume the flat fading channels in TWRC and $\phi_A = \phi_B = 0$ in (10).

A. EFFECTS OF CFO COMPENSATION

We first study how the CFO compensation approaches introduced in the preceding section affect the BER performance of the three schemes. The CFO compensation via shifting the LO frequency of relay R from $f_{o,R}$ to $f_{o,R} + \tau$ always adjusts f_{δ_A} and f_{δ_B} by the same amount of τ but keeps $\Delta\delta = \frac{f_{\delta_A} - f_{\delta_B}}{\Delta_f} = \delta_A - \delta_B$ unchanged. Given δ_A and δ_B, to see what τ is optimal for each of the schemes, we look at the BER curves of the three schemes at different (δ_A, δ_B) with $\Delta\delta = \delta_A - \delta_B$ fixed. Shown in Fig. 5 are the results for $\Delta\delta = 0.2$ and $\Delta\delta = 0.3$ at SNR $= -2$ dB (defined as $-10\log\sigma^2$). The iterative message passing in each scheme is executed for 20 rounds. We have the following observations from Fig. 5.

First, for either $\Delta\delta = 0.2$ or $\Delta\delta = 0.3$, the BER curve of each scheme is symmetric with respect to $\delta_A = -\delta_B = \frac{\Delta\delta}{2}$, and the optimal/lowest BER is achieved at $\delta_A = -\delta_B = \frac{\Delta\delta}{2}$. This demonstrates that the mean-valued (MV) compensation approach that sets $\tau = \frac{f_{\delta_A} + f_{\delta_B}}{2}$ and thus yields $\delta_A = -\delta_B = \frac{\Delta\delta}{2}$ is BER-optimal for all the three schemes. The reason is that the BER at relay R in PNC is dominated by the uplink with lower quality [17]. Specifically, as δ_A increases (decreases) from $\frac{\Delta\delta}{2}$, the received constellation of the desired signal from node A (node B) becomes more condensed (as can be seen from (10)), and thus, the probability evaluation in (20) becomes more error-prone. This eventually deteriorates the BER of each scheme. Second, Scheme 1 is superior over Schemes 2 and 3 in general. This superiority is down to the unified treatment of the ICI and the channel code within one framework like Fig. 3 in Scheme 1; however, this comes at the cost of a higher decoding complexity for Scheme 1. Notably, Scheme 3 performs rather poorly. This is because the output $\Pr(u_A^n \oplus u_B^n | y_{R,l}^k \forall l, k)$ of the detector, compared with the output $\Pr(u_A^n, u_B^n | y_{R,l}^k \forall l, k)$, generally loses information [12], which is detrimental to the decoding of X_R.

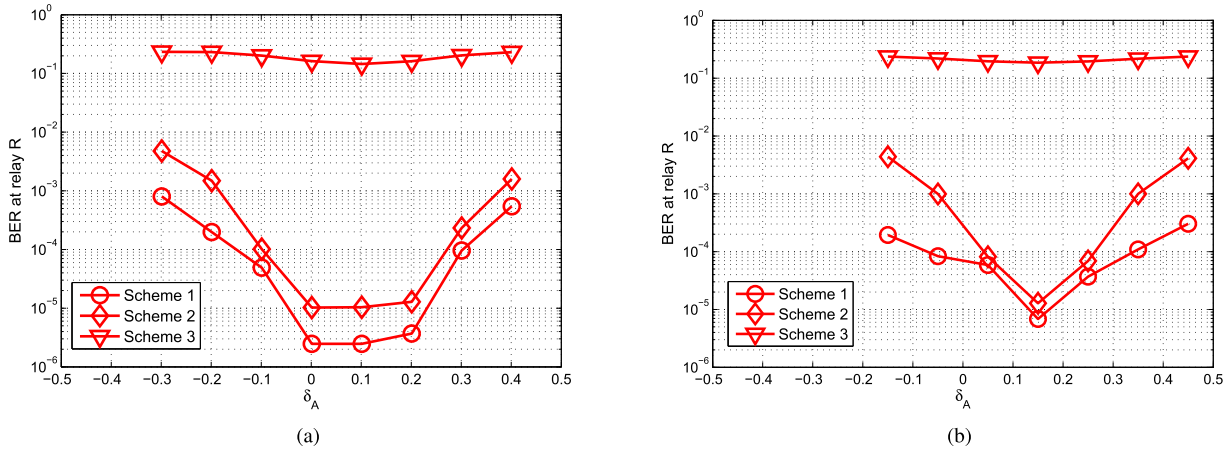

FIGURE 5. CFO effects on the BER of the three schemes at relay R for different $\Delta\delta$ (SNR = -2 dB and 20 iterations of decoding). (a) $\Delta\delta = 0.2$. (b) $\Delta\delta = 0.3$.

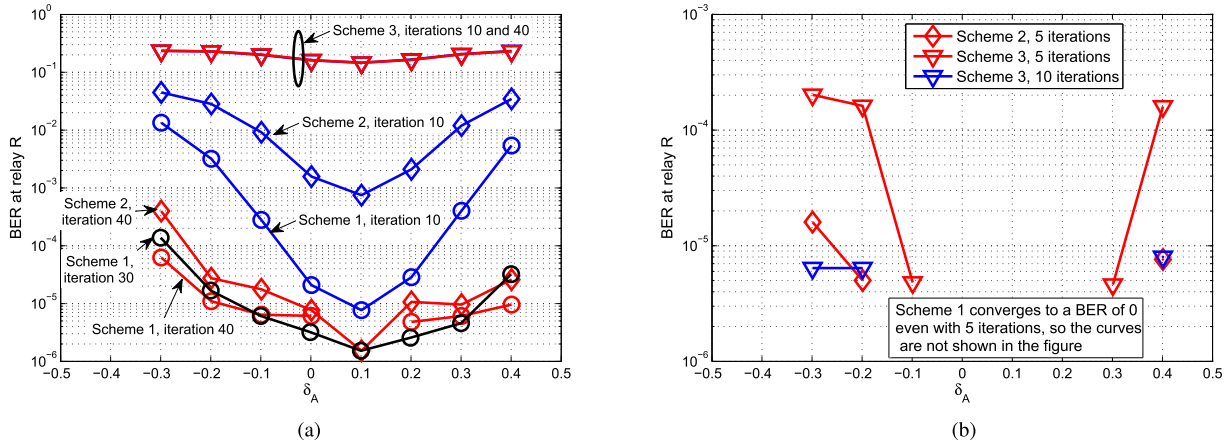

FIGURE 6. Effects of the number of iterations on the BER of the three schemes for different SNR values. (a) SNR = −2 dB. (b) SNR = 5 dB.

B. EFFECTS OF THE NUMBER OF ITERATIONS

We now study how the number of iterations of the message passing affects the three schemes. We keep the same settings as in Fig. 5 but vary the iteration rounds to see its effects. Fig. 6 shows the responses of the three schemes for two different SNR values. We see from the figure that at a low SNR value, e.g., −2 dB, more iterations improve the BER of Schemes 1 and 2 except Scheme 3, and that at a high SNR value, e.g., 5 dB, a quick convergence to a low BER can be seen for all the three schemes. At low (high) SNR levels, the messages $U_5^{m,m}$ in (20) are more (less) error-prone, resulting in more (fewer) iterations needed for probability convergence in the three schemes. Particularly, we also see that with more iterations, Scheme 2 performs close to Scheme 1. This means that for a target BER, e.g., 10^{-5}, Scheme 2 may outperform Scheme 1 in terms of the overall message passing complexity.

C. EFFECTS OF SNR

For this study, the MV CFO compensation is applied at relay R, and the iteration number is fixed at 20. Fig. 7 plots how the three schemes respond to SNR for two different $\Delta\delta$ values. Fig. 7 includes another two schemes for comparison, i.e., the traditional point-to-point communications and Gaussian-interference physical-layer network coding (GI-PNC) [4], [8], [18]. They serve as the upper bound and lower bound for Schemes 1, 2, and 3, respectively. The former is concerned with the BER of the uplink from one end node in TWRC, assuming that the same RA code with repeat factor $q = 3$ is used at the end node and the CFO of the uplink is eliminated at relay R. The latter treats the ICI in (10) as Gaussian noise to first compute $\Pr(u_{A,l}^m \oplus u_{B,l}^m | y_{R,l}^m)$ and then channel-decode $X_R = X_A \oplus X_B$ using message passing as done in Scheme 3. Note that no message passing is needed for the computation of $\Pr(u_{A,l}^m \oplus u_{B,l}^m | y_{R,l}^m)$.

We have the following observations from Fig. 7. First, Scheme 1 is still the best performer among the three proposed schemes for SNR ≥ -3 dB. Second, channel decoding performed on the bit pair sequence $(u_{A,l}^m, u_{B,l}^m)$ in PNC is advantageous, compared with that on the XORed bit sequence $(u_{A,l}^m \oplus u_{B,l}^m)$. This is because XORing $u_{A,l}^m$ and $u_{B,l}^m$ generally leads to information loss and then undermines the decoding

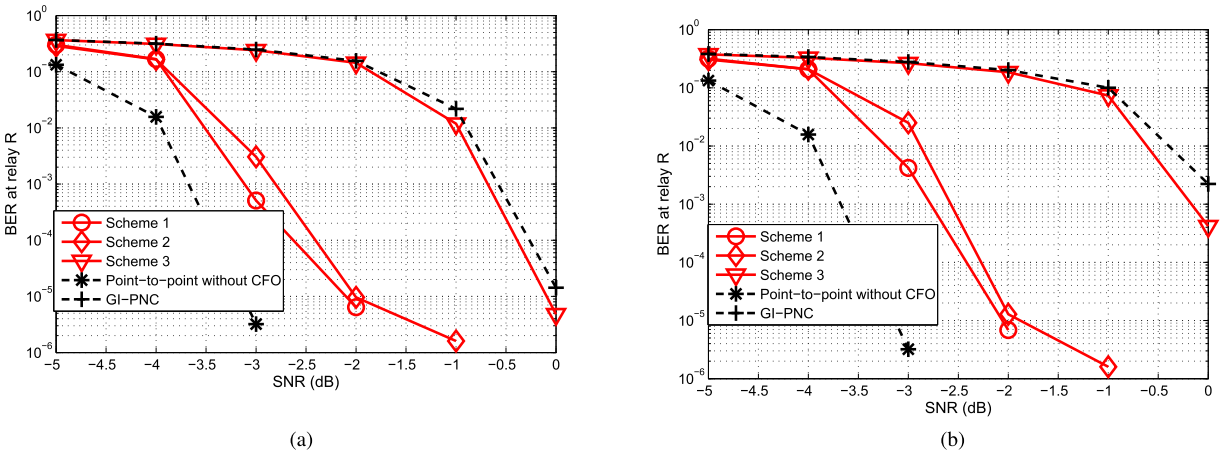

FIGURE 7. Effects of SNR on the BER of the three schemes for different $\Delta\delta$ values. (a) $\Delta\delta = 0.2$. (b) $\Delta\delta = 0.3$.

of X_R [12]. Third, more importantly, for a target BER of 10^{-5} in both Figs. 7(a) and (b), Schemes 1 and 2, compared with the point-to-point communications in the ideal case (i.e., without CFO), lag behind for only about 1 dB of SNR. This means that for low to medium levels of δ_A and δ_B with $|\Delta\delta| \leq 0.3$, we can trade about 1 dB of SNR for halved transmission times in TWRC, as PNC halves the transmission times of the point-to-point communications.

D. EFFECTS OF ϕ_i

In the above studies, $\phi_A = \phi_B = 0$ in (10) is assumed. Here, we repeat the above studies by varying ϕ_A and ϕ_B to see their effect on the three schemes. We find that for such a long OFDM frame composed of $L = 90$ OFDM symbols, the BER of the three schemes do not vary with ϕ_A or ϕ_B (not shown as figures here). The reason is as follows. Given δ_A and δ_B, [18] illustrated that for the l-th symbol, $\theta_{A,l}$ and $\theta_{B,l}$ in (20) had an impact on the probability evaluation of $U_5^{m,m}$ within one symbol, that is, some combinations of $\theta_{A,l}$ and $\theta_{B,l}$ led to a more error-prone $U_5^{m,m}$ and some led to a less error-prone $U_5^{m,m}$. This can also be seen in Schemes 1, 2, and 3, as shown in Fig. 8 where $\Delta\delta = 0.4$ and $L = 1$, i.e., an OFDM frame consists of only one OFDM symbol. We see that all the three schemes are affected by $\Delta\theta(0) = 0.4\pi + \theta_{A,0} - \theta_{B,0}$. For a long OFDM frame, however, we see from $\theta_{i,l} = \phi_i + 2\pi f_{\delta_i} l(T_s + T_g)$ in (20) that regardless of ϕ_A and ϕ_B, $\theta_{A,l}$ and $\theta_{B,l}$ (or $\Delta\theta(l)$) vary with symbols in the frame, and thus, the factor graphs of the three schemes are fed with both high-quality and low-quality messages $U_5^{m,m}$. This keeps the BER over one frame the same for different ϕ_A and ϕ_B.

In fact, we have conducted simulations to study the three schemes in the frequency-selective channel, and observed that (i) for short OFDM frames, the BER of Scheme 1, 2, or 3 keeps the same for most realizations of the random variables $\phi_{m,i}$ in (13), and (ii) for long OFDM frames, the BER of each of the three schemes is nearly the same as that in the flat fading channel. The reasons are as follows. With our proposed power control and δ_A and δ_B given, the quality of the messages $U_5^{m,m}$ under the frequency-selective channel is primarily affected by the phases $\phi_{m,i}$, and due to the varying nature of $\phi_{m,i}$ for different m and i, different message qualities do exist *even within one OFDM symbol*. This results in the observations (i) and (ii) above. Our simulations also reveal that for short OFDM frames in the frequency-selective channel, Scheme 1 still dominates in general.

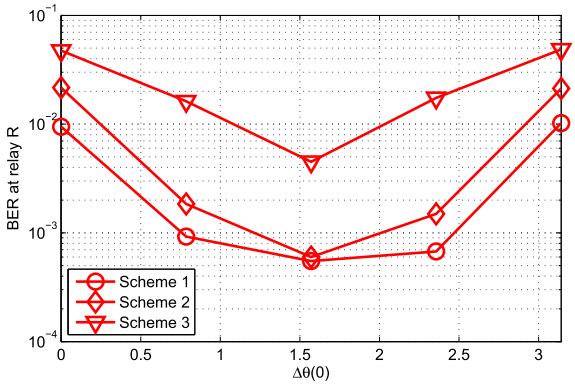

FIGURE 8. Effects of $\Delta\theta(0)$ on the BER of Schemes 1, 2 and 3 for $L = 1$, $\Delta\delta = 0.4$, and SNR = 2 dB.

VI. CONCLUSION

This paper has addressed the carrier frequency offset (CFO) problem in OFDM modulated physical-layer network coding (PNC) in a two-way relay channel (TWRC). It deals with the receiver design at the relay and puts emphasis on the functional blocks of CFO compensation, signal detection, and channel decoding for CFO effect mitigation. Multiple design choices for each block have been considered. Specifically, we have proposed one scheme for joint signal detection and channel decoding and two schemes for separate signal detection and channel decoding. For each scheme, a belief propagation or message passing algorithm(s) runs on a factor graph for probability marginalization and the XOR decoding in PNC. These three schemes can be applied under both the

flat fading channel and the frequency-selective channel. For the CFO compensation, which precedes the other two blocks, we have considered the approaches that differ from each other in the adjusted amount of the CFO for both end nodes in TWRC.

We have conducted extensive simulations for repeat-accumulate (RA) coded PNC. We find that the mean-valued (MV) CFO compensation approach that yields opposite CFO values of the two uplinks in TWRC is a good match for all the three schemes. We also find that with power control at the end nodes, each of the three schemes performs the same under both the flat fading channel and the frequency-selective channel. More importantly, we have shown that for a target BER of 10^{-5} at low to medium CFO level of the two uplinks, the joint scheme, the best performer among the three, lags behind the point-to-point communications without CFO for only about 1 dB. This exhibits PNC as a promising performance booster in TWRC.

For future work, we attempt to extend our schemes to higher-order modulations such as QPSK modulation. The XOR decoding in PNC usually becomes complicated under a higher-order modulation [19], and to investigate the BER performance gap between our proposed schemes and the point-to-point communications will be of interest. Also, we attempt to explore effective power control for our schemes in scenarios where deep fading occurs. Given a total power limit at one end node, a desirable power control scheme will take the subcarrier suppression into consideration.

APPENDIX
MESSAGE UPDATE RULES IN SCHEME 1

This appendix illustrates how messages are composed in some steps of the message passing for Scheme 1.

In step 2, the messages pertaining to symbol $l = 0$ and to be updated from left to right are $M_1^{k,k}$ and $M_2^{k,k+1}$, $0 \le k \le K-2$, and they are composed as follows

$$M_1^{k,k} = f_k \cdot M_2^{k-1,k} \cdot D_4^{k,k} \cdot D_4^{k+1,k}, \tag{25}$$

and

$$M_2^{k,k+1}(u_A^{k+1,k}, u_B^{k+1,k+2}) = \sum_{u_A^{k-1}, u_B^k} M_1^{k,k}(u_A^{k,k-1}, u_B^{k,k+1}). \tag{26}$$

In (25), $M_2^{k-1,k}$ is not applicable for $k = 0$. Similarly, the messages $M_1^{k,k-1}$ and $M_2^{k-1,k-1}$ $(1 \le k \le K-1)$ to be updated from right to left are composed as follows

$$M_1^{k,k-1} = f_k \cdot M_2^{k,k} \cdot D_4^{k,k} \cdot D_4^{k+1,k}, \tag{27}$$

and

$$M_2^{k-1,k-1}(u_A^{k-1,k-2}, u_B^{k-1,k}) = \sum_{u_A^k, u_B^{k+1}} M_1^{k,k-1}(u_A^{k,k-1}, u_B^{k,k+1}). \tag{28}$$

In (27), $M_2^{k,k}$ is not applicable for $k = K-1$.

In step 3, the upward messages $U_4^{m,m}$ and $U_4^{m,m+1}$ $(0 \le m \le N-1)$ are composed as follows

$$U_4^{m,m} = D_4^{m+1,m} \cdot f_m \cdot M_2^{m-1,m} \cdot M_2^{m,m}, \tag{29}$$

and

$$U_4^{m,m+1} = D_4^{m,m} \cdot f_m \cdot M_2^{m-1,m} \cdot M_2^{m,m}. \tag{30}$$

In (29), $D_4^{m+1,m}$ is not applicable for $m = N-1$. Also, in both (29) and (30), $M_2^{m-1,m}$ $(M_2^{m,m})$ is not applicable for $m \pmod K = 0$ (for $m \pmod K = K-1$).

In step 4, the upward messages $U_3^{0,0}$ is given by

$$U_3^{0,0}(\tilde{x}_A^0, \tilde{x}_B^0) = \sum_{\tilde{U}_0 : u_A^0 = \tilde{x}_A^0, u_B^0 = \tilde{x}_B^0} U_4^{0,0}(\underbrace{u_A^{0,-1}, u_B^{0,1}}_{=\tilde{U}_0}). \tag{31}$$

To compose $U_3^{m,m}$, $1 \le m \le N-1$, here we consider a possible definition of β_m, that is, $\beta_m = 1$ occurs only in the following conditions: from $\tilde{U}_m$, u_A^m and u_A^{m-1} satisfy $u_A^{m-1} \oplus u_A^m = \tilde{x}_A^m$, and from $\tilde{U}_{m-1}$, u_B^m and u_B^{m-1} satisfy $u_B^{m-1} \oplus u_B^m = \tilde{x}_B^m$. Then, $U_3^{m,m}(\tilde{x}_A^m, \tilde{x}_B^m)$ is the product of the following two quantities/functions

$$Q_1(\tilde{x}_B^m) = \sum_{\tilde{U}_{m-1} : u_B^{m-1} \oplus u_B^m = \tilde{x}_B^m} U_4^{m-1,m}(\underbrace{u_A^{m-1,m-2}, u_B^{m-1,m}}_{=\tilde{U}_{m-1}});$$
$$Q_2(\tilde{x}_A^m) = \sum_{\tilde{U}_m : u_A^{m-1} \oplus u_A^m = \tilde{x}_A^m} U_4^{m,m}(\underbrace{u_A^{m,m-1}, u_B^{m,m+1}}_{=\tilde{U}_m}). \tag{32}$$

In step 6, the downward message $D_1^{m,n}$, $m \cdot q \le n \le (m+1) \cdot q - 1$, is updated as follows

$$D_1^{m,n} = \prod_{k=m \cdot q, k \ne n}^{(m+1) \cdot q - 1} U_1^{k,m}. \tag{33}$$

In step 7, the downward message $D_4^{0,0}$ is given by

$$D_4^{0,0}(u_A^{0,-1}, u_B^{0,1}) = D_3^{0,0}(\tilde{x}_A^0 = u_A^0, \tilde{x}_B^0 = u_B^0). \tag{34}$$

For $m > 0$, the messages $D_4^{m,m}$ and $D_4^{m,m-1}$ are respectively given by

$$D_4^{m,m}(u_A^{m,m-1}, u_B^{m,m+1}) = \sum_{\tilde{x}_B^m} D_3^{m,m}(\tilde{x}_A^m = u_A^{m-1} \oplus u_A^m, \tilde{x}_B^m) \cdot Q_1(\tilde{x}_B^m), \tag{35}$$

and

$$D_4^{m,m-1}(u_A^{m-1,m-2}, u_B^{m-1,m}) = \sum_{\tilde{x}_A^m} D_3^{m,m}(\tilde{x}_A^m, \tilde{x}_B^m = u_B^{m-1} \oplus u_B^m) \cdot Q_2(\tilde{x}_A^m). \tag{36}$$

REFERENCES

[1] S. Zhang, S. C. Liew, and P. P. Lam, "Physical-layer network coding," in *Proc. MobiCom*, 2006, pp. 358–365.

[2] S. Zhang, S.-C. Liew, and H. Wang, "Synchronization analysis for wireless TWRC operated with physical-layer network coding," *Wireless Pers. Commun.*, vol. 68, no. 3, pp. 647–653, 2013.

[3] Y. Shao, S.-C. Liew, and L. Lu, "Asynchronous physical-layer network coding: Symbol misalignment estimation and its effect on decoding," *IEEE Trans. Wireless Commun.*, vol. 16, no. 10, pp. 6881–6894, Oct. 2017.

[4] L. Lu, T. Wang, S.-C. Liew, and S. Zhang, "Implementation of physical-layer network coding," *Phys. Commun.*, vol. 6, pp. 74–87, Mar. 2013.

[5] I. W.-H. Ho, S.-C. Liew, and L. Lu, "Feasibility study of physical-layer network coding in 802.11 p VANETs," in *Proc. IEEE ISIT*, Jun. 2014, pp. 646–650.

[6] L. F. Xie, I. W.-H. Ho, S.-C. Liew, L. Lu, and F. C. M. Lau, "Mitigating Doppler effects on physical-layer network coding in VANET," in *Proc. IEEE PIMRC*, Aug. 2015, pp. 121–126.

[7] Z. Wang, J. Huang, S. Zhou, and Z. Wang, "Iterative receiver processing for OFDM modulated physical-layer network coding in underwater acoustic channels," *IEEE Trans. Commun.*, vol. 61, no. 2, pp. 541–553, Feb. 2013.

[8] M. Wu, F. Ludwig, M. Woltering, D. Wübben, A. Dekorsy, and S. Paul, "Analysis and implementation for physical-layer network coding with carrier frequency offset," in *Proc. ITG WSA*, 2014, pp. 1–8.

[9] Y. Li and L. J. Cimini, "Bounds on the interchannel interference of OFDM in time-varying impairments," *IEEE Trans. Commun.*, vol. 49, no. 3, pp. 401–404, Mar. 2001.

[10] T. Wang, J. G. Proakis, E. Masry, and J. R. Zeidler, "Performance degradation of OFDM systems due to Doppler spreading," *IEEE Trans. Wireless Commun.*, vol. 5, no. 6, pp. 1422–1432, Jun. 2006.

[11] S. Katti, H. Rahul, W. Hu, D. Katabi, M. Medard, and J. Crowcroft, "XORs in the air: Practical wireless network coding," in *Proc. ACM SIGCOMM*, 2006, pp. 243–254.

[12] S. C. Liew, S. Zhang, and L. Lu, "Physical-layer network coding: Tutorial, survey, and beyond," *Phys. Commun.*, vol. 6, pp. 4–42, Mar. 2013.

[13] L. Lu, L. You, and S. C. Liew, "Network-coded multiple access," *IEEE Trans. Mobile Comput.*, vol. 13, no. 12, pp. 2853–2869, Dec. 2014.

[14] L. You, S. C. Liew, and L. Lu, "Network-coded multiple access II: Toward real-time operation with improved performance," *IEEE J. Sel. Areas Commun.*, vol. 33, no. 2, pp. 264–280, Feb. 2015.

[15] M. Park, I. Choi, and I. Lee, "Exact BER analysis of physical layer network coding for two-way relay channels," in *Proc. IEEE VTC*, May 2011, pp. 1–5.

[16] Y. Huang, S. Wang, Q. Song, L. Guo, and A. Jamalipour, "Synchronous physical-layer network coding: A feasibility study," *IEEE Trans. Wireless Commun.*, vol. 12, no. 8, pp. 4048–4057, Aug. 2013.

[17] T. Koike-Akino, P. Popovski, and V. Tarokh, "Optimized constellations for two-way wireless relaying with physical network coding," *IEEE J. Sel. Areas Commun.*, vol. 27, no. 5, pp. 773–787, Jun. 2009.

[18] L. F. Xie, I. W.-H. Ho, S.-C. Liew, L. Lu, and F. C. M. Lau, "The feasibility of mobile physical-layer network coding with BPSK modulation," *IEEE Trans. Veh. Technol.*, vol. 66, no. 5, pp. 3976–3990, May 2017.

[19] L. Lu and S. C. Liew, "Asynchronous physical-layer network coding," *IEEE Trans. Wireless Commun.*, vol. 11, no. 2, pp. 819–831, Feb. 2012.

[20] M. Woltering, D. Wubben, and A. Dekorsy, "Physical layer network coding with Gaussian waveforms using soft interference cancellation," in *Proc. VTC Spring*, May 2015, pp. 1–5.

[21] T. Wang and S. C. Liew, "Joint channel estimation and channel decoding in physical-layer network coding systems: An EM-BP factor graph framework," *IEEE Trans. Wireless Commun.*, vol. 13, no. 4, pp. 2229–2245, Apr. 2014.

[22] S. Brink and G. Kramer, "Design of repeat-accumulate codes for iterative detection and decoding," *IEEE Trans. Signal Process.*, vol. 5, no. 11, pp. 2764–2772, Nov. 2003.

[23] T. Lv, H. Li, and J. Chen, "Joint estimation of symbol timing and carrier frequency offset of OFDM signals over fast time-varying multipath channels," *IEEE Trans. Signal Process.*, vol. 53, no. 12, pp. 4526–4535, Dec. 2005.

[24] J. Yedidia, W. Freeman, and Y. Weiss, "Understanding belief propagation and its generalizations," MERL, Cambridge, MA, USA, Tech. Rep. TR2001-22, 2001.

[25] *IEEE Standard for Information Technology—Local and Metropolitan Area Networks—Specific Requirements—Part 11: Wireless LAN MAC and PHY Specifications Amendment 6—Wireless Access in Vehicular Environments*, IEEE Standard 802.11, 2010.

[26] G. Bartoli, R. Fantacci, D. Marabissi, and R. Simoni, "Subcarriers suppression methods for OFDM systems with decode-and-forward network coding," *IEEE Trans. Wireless Commun.*, vol. 12, no. 12, pp. 6034–6042, Dec. 2013.

[27] M. Stojanovic, "Low complexity OFDM detector for underwater acoustic channels," in *Proc. IEEE OCEANS*, Sep. 2006, pp. 1–6.

[28] "Practical manufacturing testing of 802.11 OFDM wireless devices," LittlePoint, Sunnyvale, CA, USA, White Paper 1075-0407-001, 2012. [Online]. Available: http://www.litepoint.com/wp-content/uploads/2014/02/Testing-802.11-OFDM-Wireless-Devices_WhitePaper-1.pdf

[29] S. Zhang and S.-C. Liew, "Channel coding and decoding in a relay system operated with physical-layer network coding," *IEEE J. Sel. Areas Commun.*, vol. 27, no. 5, pp. 788–796, Jun. 2009.

LING FU XIE received the B. Eng. and M. Eng. degrees in communications engineering from the University of Electronic Science and Technology of China in 2006 and 2009, respectively, and the Ph.D. degree from Nanyang Technological University, Singapore, in 2014. From 2014 to 2015, he was a Post-Doctoral Fellow with The Hong Kong Polytechnic University, Hong Kong. In 2015, he joined the Faculty of Electrical Engineering and Computer Science, Ningbo University, Ningbo, China. His research interests mainly include protocol design and performance analysis in mobile networks, wireless network coding, and physical-layer network coding.

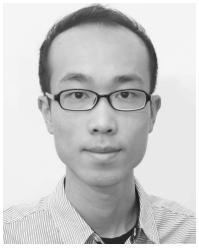

IVAN WANG-HEI HO received the B.Eng. and M.Phil. degrees in information engineering from The Chinese University of Hong Kong, Hong Kong, in 2004 and 2006, respectively, and the Ph.D. degree in electrical and electronic engineering from Imperial College London, London, U.K., in 2010. He was with the Mobile Environmental Sensing System Across a Grid Environment Project funded by the Engineering and Physical Sciences Research Council and the Department for Transport of the U.K., and with the International Technology Alliance Project funded by the U.S. Army Research Laboratory and the Ministry of Defence of U.K., during his Ph.D. degree. In 2007, he was with the IBM Thomas J. Watson Research Center, Hawthorne, NY, USA. After his Ph.D. degree, he was with the System Engineering Initiative, Imperial College London, as a Post-Doctoral Research Associate. In 2010, he co-founded P2 Mobile Technologies Ltd., Hong Kong Science Park, and served as a Chief Research and Development Engineer. He is currently a Research Assistant Professor with the Department of Electronic and Information Engineering, The Hong Kong Polytechnic University, Hong Kong. He holds a U.S. patent. His research interests include wireless communications and networking, specifically in vehicular ad hoc networks and intelligent transportation systems, physical-layer network coding, and wireless mesh networks. He primarily invented the MeshRanger series wireless mesh embedded system, which received the Silver Award in Best Ubiquitous Networking from the Hong Kong ICT Awards 2012. His publications can be found at http://www.eie.polyu.edu.hk/∼whho.

ZHEN HUI SITU received the B.S. degree in electronic information science and technology from Sun Yat-sen University, Guangzhou, China, and the M.Sc. degree in electronic engineering from The Hong Kong University of Science and Technology, Hong Kong, where he is currently pursuing the Ph.D. degree with the Department of Electronic and Information Engineering. From 2014 to 2015, he was a Research Assistant with The Hong Kong Polytechnic University. His research interests include wireless communications and statistical signal processing, specifically in vehicular ad hoc networks (VANET). His most research focus is on the feasibility study of physical-layer network coding in VANETs.

LU LU received the B.E. degree from the University of Science and Technology of China in 2007 and the Ph.D. degree from The Chinese University of Hong Kong (CUHK) in 2012. From 2012 to 2014, he was a Post-Doctoral Fellow with the Institute of Network Coding, CUHK, where he was a Research Assistant Professor from 2014 to 2017. He is currently a Professor with the Technology and Engineering Center for Space Utilization, Chinese Academy of Sciences. His research interests include wireless and optical communications, multi-user detection, physical-layer network coding, and software-defined radio. He was a recipient of the Faculty's Outstanding Ph.D. Thesis Award and the Postgraduate Research Output Award both in 2013 at CUHK.

WEIDANG LU received the Ph.D. degree in information and communication engineering from the Harbin Institute of Technology in 2012. He was a Visiting Scholar with Nanyang Technology University, Singapore, The Chinese University of Hong Kong, China, and the Southern University of Science and Technology, China. He is currently an Associate Professor with the College of Information Engineering, Zhejiang University of Technology, Hangzhou, China. His current research interests include simultaneous wireless information and power transfer, wireless sensor networks, cooperative communications, and physical-layer security for wireless systems.